One-Dimensional Analysis of Liquid-Fueled Combustion Instability

R. Bhatia* and W. A. Sirignano†
University of California, Irvine, Irvine, California 92717

A one-dimensional computational analysis is performed to investigate the liquid-fueled combustion instability. The governing gas-phase equations in an Eulerian frame are solved using an implicit scheme based on the implicit continuous-fluid Eulerian (ICE) method. The liquid-phase equations in a Lagrangian frame are solved using the Effective Conductivity Model. Dirichlet boundary conditions are imposed at the combustor inlet, with a time-dependent inlet gas velocity. Neumann boundary conditions with the short-nozzle approximation are employed at the outlet. Spray characteristics, mixture ratio profiles, and combustor geometry are amongst the parameters studied. Both stable and unstable modes of combustor operation are found. Under certain conditions, limited cycle behavior of pressure, temperature, and velocity oscillations is obtained. The frequency of oscillation is approximately the fundamental resonant frequency of a chamber with one closed end and one open end, and is independent of the forcing function frequency. Large-scale temperature or entropy waves convected with the gas velocity are seen for some cases. The parameter domains of stable/unstable combustor operation have been plotted. Vaporization is rate controlling and the ratio of the period of oscillation to droplet heating time and the ratio of residence time to droplet heating time emerge as important parameters.

Nomenclature

a = speed of sound
C_D = drag coefficient
C_p = specific heat
$\mathcal{D}$ = mass diffusivity
d = droplet diameter
E_A = activation energy
Eu = Euler number
L = latent heat of evaporation, combustor length
$\overline{M}$ = average molecular weight of the gas-phase
$\dot{m}_l$ = mass vaporization rate
n = number of droplets
OER = overall equivalence ratio
p = pressure
Q = artificial viscosity
q = heat of combustion
Re = Reynolds number
r = droplet radius
S = source term in gas-phase equations
T = temperature
t = time
u = velocity
W_{CH} = reaction rate
x = distance
Y = mass fraction
α = stoicliometric coefficient
β = viscosity coefficient
γ = specific heat ratio
λ = thermal conductivity
ρ = gas-phase density
τ = artificial diffusivity coefficient, characteristic time

Subscripts

f = fuel
g = gas-phase
i = species i
k = kth droplet group
l = liquid-phase
n = inert
o = oxidant

Superscripts

$'$ = dimensional variable
$*$ = reference variable

Introduction

COMBUSTION instability is an important issue in the development of liquid-fueled combustors and there exists considerable incentive to seek a better understanding of this phenomenon. In general terms, the combustion instability results from the coupling between the combustion and the fluid dynamics of the system. Combustion of fuel vapor provides oscillatory energy input through this coupling. The oscillations can decay if the damping processes are sufficiently large to dissipate the oscillatory energy more rapidly than it is supplied. The rate of combustion in liquid-fueled ramjets is controlled by the vaporization rate of the fuel spray which is dependent on the spray characteristics, properties of the fuel, heat and mass transfer rates, etc.

In the time lag theory, developed by Crocco,[1] the overall time lag from the injection to vaporization and combustion is used to predict instability occurrences. The efforts of the rocket research society are reviewed in Harrje and Reardon.[2] Other earlier studies[3–6] concentrated on analytically studying the vaporization as a rate-controlling mechanism for instability. Either the liquid thermal inertia was treated as infinite,[2–4] or the liquid temperature was assumed uniform throughout the droplet interior.[2,5,6] This led to overestimation of the thermal inertia of the liquid. These studies did not provide convincing evidence of vaporization as the driving mechanism for the instability. Since then, great progress has been made in treatment of transient heating and vaporization of the fuel droplets in air-breathing combustors.[7] Recently, Tong and Sirignano[8] examined the response of a vaporizing droplet to oscillating ambient pressure and velocity conditions. They report a substantial oscillatory response of the vaporization rate. However, the liquid droplet vaporization

Presented as Paper AIAA-90-0271 at the AIAA 28th Aerospace Sciences Meeting, Reno, NV, Jan. 8–11, 1990; received Feb. 26, 1990; revision received Aug. 27, 1990; accepted for publication Aug. 28, 1990.

*Research Assistant, Department of Mechanical and Aerospace Engineering. Member AIAA.

†Professor, Department of Mechanical and Aerospace Engineering. Fellow AIAA.

model used there is strictly limited to high droplet Reynolds number and becomes inaccurate as the relative droplet-gas velocity decreases to small values or changes sign. There has been renewed effort to understand the mechanism of combustion instability in liquid-fueled systems. Amongst these are the efforts of: Culick et al.[9-11]; Kailasanath et al.[12]; and Hedge et al.[13]

Many authors[9,11-13] have considered the interaction of vortex structures and acoustic waves to be the dominant mechanism in ramjet combustion instability. Some experimental and theoretical evidence points to the plausibility of this mechanism. However, that research excludes a priori the role of spray combustion by considering gaseous fuels. In practice, there is substantial scientific reason to believe that the relatively crude fuel injection system of a ramjet results in spray vaporization becoming a controlling factor. For example, spray vaporization is found to be controlling in other combustion systems with much more sophisticated fuel injection and atomization. This study is an attempt to examine the importance of spray vaporization in an oscillatory combustion situation.

The objective of this computational study is to gain fundamental understanding of the effects of various design parameters on the stability of the combustion process in liquid-fueled systems. The inlet conditions do not relate precisely to a practical combustor. However, our model system has the general characteristics of a liquid-fueled ramjet and general conclusions drawn from these calculations should apply to ramjets. Spray characteristics, mixture ratio profiles, and combustor geometry are amongst the more interesting parameters investigated. Effort has concentrated on the unsteady solution for the gas and liquid phases, evaluation of the effects of inlet gas velocity perturbations, and the coupling between gas and liquid phases under perturbed conditions. The present study is limited to one-dimensional fluid mechanics and longitudinal instabilities only.

The one-dimensional, unsteady, compressible flow is described by Eulerian gas-phase conservation equations, and Lagrangian liquid-phase equations which are based on Abramzon and Sirignano.[14] This liquid-phase model has the advantage of remaining valid for lower values of droplet Reynolds number including the situation where the relative gas-droplet velocity changes sign. The gas-phase conservation equations are solved using a modified Implicit Continuous-fluid Eulerian (ICE) method due to Harlow et al.[15] and Westbrook and Chase.[16] Dirichlet boundary conditions are used at the combustor inlet, and, at the outlet, Neumann boundary conditions along with the short-nozzle approximation are specified. The details of the formulation and the solution method are presented in the following sections.

Physical Model and Formulation

The physical model studied is a simplified, one-dimensional approximation of a ramjet combustion chamber (Fig. 1) in which vaporization and combustion of liquid spray occurs. Monodispersed, monocomponent liquid spray is assumed. The gas-phase is taken as unsteady, subsonic, compressible, and exchanges mass, momentum, and heat transfer with the liquid-phase. The basic set of equations in the Eulerian approach[16] includes continuity, momentum, chemical species, energy and an equation of state for the gas phase. The nondimensional set of gas-phase equations is summarized below, along with source terms for each equation, which model the interaction between the gas and the liquid phases. Here, the variables are nondimensionalized by reference length (L^*), velocity (u^*), time ($t^* = L^*/u^*$), pressure (p^*), temperature (T^*), density ($\rho^* = p^*/R_u T^*$), and specific heat (C_p^*)

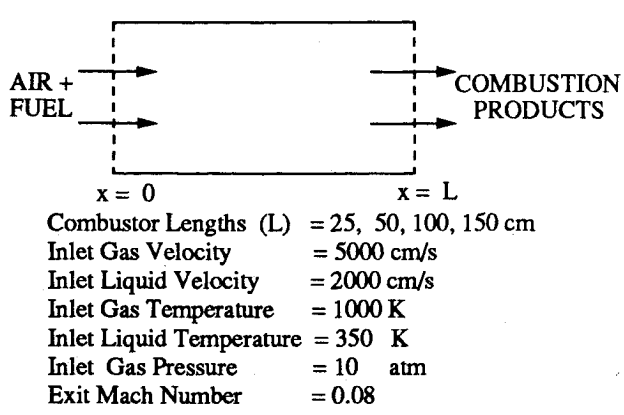

Fig. 1 Physical model of the combustor.

$$\frac{\partial \rho}{\partial t} + \frac{\partial}{\partial x}(\rho u) = \frac{\partial}{\partial x}\left(\tau \frac{\partial \rho}{\partial x}\right) + S_\rho \tag{1}$$

$$\frac{\partial}{\partial t}(\rho u) + \frac{\partial}{\partial x}(\rho u^2) = -Eu \frac{\partial}{\partial x}(p + Q) + S_u \tag{2}$$

$$\frac{\partial T}{\partial t} + u \frac{\partial T}{\partial x} = \left(1 - \frac{1}{\gamma^*}\right) \frac{1}{\rho C_p} \cdot \left(\frac{\partial p}{\partial t} + u \frac{\partial p}{\partial x}\right) + \frac{1}{\rho C_p} \frac{\partial}{\partial x}\left(\lambda_g \frac{\partial T}{\partial x}\right) + S_T \tag{3}$$

$$\frac{\partial}{\partial t}(\rho Y_i) + \frac{\partial}{\partial x}(\rho Y_i u) = \frac{\partial}{\partial x}\left(\rho \mathcal{D} \frac{\partial Y_i}{\partial X}\right) + S_{Y_i} \tag{4}$$

$$p = \rho T/\bar{M} \tag{5}$$

where τ is artificial diffusivity coefficient[15] and Q is artificial viscosity.[16] In all of our calculations, the artificial diffusivity and viscosity coefficients are set to zero. Further, we have

$$Q = -\beta \frac{\partial u}{\partial x} \tag{6}$$

$$Eu = p^*/(\rho^* u^{*2}) \tag{7}$$

$$S_\rho = \frac{L^* t^*}{\rho^*}\left[\frac{1}{\Delta x'}(n_k' m_k')\right] \tag{8}$$

$$S_u = \frac{L^* t^*}{\rho^* u^*}\left[\frac{1}{\Delta x'} n_k' m_k'(u_k' - u_g') + \frac{1}{\Delta x'}\frac{1}{2}\rho_g' \pi \frac{d_k'^2}{4} C_{Dk}(u_k' - u_g')|(u_k' - u_g')|\right] \tag{9}$$

$$S_T = \frac{1}{\rho C_p}\frac{t^*}{\rho^* C_p^* T^*}(Q_{\text{combustion}} - Q_{\text{drop heating}} - Q_{\text{evaporation}} - Q_{\text{vapor heating}}) \tag{10}$$

$$Q_{\text{combustion}} = q' M_f' W_{CH}' \tag{11}$$

$$Q_{\text{drop heating}} = \frac{L^*}{\Delta x'} n_k' 4\pi r_k'^2 \lambda_l' \frac{\partial T_{l,k}'}{\partial r'}\Big|_{r_{sk}} \tag{12}$$

$$Q_{\text{evaporation}} = \frac{L^*}{\Delta x'} n_k' m_k' L_{\text{evaporation}}' \tag{13}$$

$$Q_{\text{vapor heating}} = \frac{L^*}{\Delta x'} n_k' m_k' C_{pf,g}(T_g' - T_{sk}') \tag{14}$$

$$S_{Y_f} = \frac{t^*}{\rho^*}\left(\frac{L^*}{\Delta x'} n_k' m_k' - M_f' W_{CH}'\right) \tag{15}$$

$$S_{Y_o} = \frac{t^*}{\rho^*}(-\alpha_{st}M_o'W_{CH}') \tag{16}$$

$$S_{Y_n} = \frac{t^*}{\rho^*}(\alpha_n M_o'W_{CH}') \tag{17}$$

The Lagrangian formulation of the liquid-phase equations is based on the Effective Conductivity Model.[14] This droplet model assumes quasi-steadiness in the gas film and employs the one-third-averaging rule to evaluate the gas-mixture properties. The assumptions of unity Lewis and Prandtl numbers have been removed. The effect of Stefan flow on the heat and mass transfer is modeled by a correction on the film thickness. For efficient computational time and accuracy, an "effective" value of the liquid thermal conductivity is used to account for the internal circulation within the droplet. Note that the vaporization model accounts for the droplet drag and the heat and mass transfer with the gas-phase. The equations are summarized here.[17] The droplet trajectory is given by

$$\frac{dx}{dt} = U_l \tag{18}$$

where x is the position of the center of the droplet, and U_l is the droplet velocity given by

$$\frac{dU_l}{dt} = \frac{3}{16}\frac{\mu}{\rho_l}\frac{(U - U_l)}{r_l^2}ReC_D \tag{19}$$

$$Re = \frac{2\rho|U - U_l|r_l}{\mu} \tag{20}$$

$$C_D = \frac{24}{Re}\left[1 + \frac{Re^{2/3}}{6}\right] \tag{21}$$

The droplet radius is governed by

$$\frac{dr_l}{dt} = -\dot{m}_l/(4\pi\rho_l r_l^2) \tag{22}$$

The instantaneous droplet vaporization rate is given by

$$\dot{m}_l = 2\pi\bar{\rho}_g\bar{\mathcal{D}}_g r_l Sh\,\ln(1 + B_M) \tag{23}$$

The Sherwood number for a nonvaporizing sphere is[18]

$$Sh_0 = 1 + (1 + ReSc)^{1/3}f(Re) \tag{24}$$

where $f(Re) = 1$ at $Re \le 1$ and $f(Re) = Re^{0.077}$ at $1 < Re \le 400$. To account for Stefan flow due to droplet regression, the modified Sherwood number is calculated as

$$Sh = 2 + (Sh_0 - 2)/F_M \tag{25}$$

where the correction factor is given by

$$F_M = (1 + B_M)^{0.7}\frac{\ln(1 + B_M)}{B_M} \tag{26}$$

The mass transfer number is calculated as

$$B_M = \frac{Y_{fs} - Y_{f\infty}}{1 - Y_{fs}} \tag{27}$$

Heat transfer inside the droplet is governed by the transient heat conduction equation for the spherically symmetric droplets

$$\frac{\partial T}{\partial t} = \frac{1}{\rho_l C_{pl} r^2}\frac{\partial}{\partial r}\left(\lambda_{\text{eff}} r^2 \frac{\partial T}{\partial r}\right) \tag{28}$$

with the boundary conditions

$$\text{at the droplet center, } r = 0;\ \frac{\partial T}{\partial r} = 0 \tag{29}$$

$$\text{at the droplet surface, } r = r_l(t);\ \frac{\partial T}{\partial r} = \frac{Q_l}{4\pi\lambda_l r_l(t)^2} \tag{30}$$

The effective liquid conductivity is given as a function of the liquid Peclet number

$$\frac{\lambda_{\text{eff}}}{\lambda_l} = 1.86 + \tanh\left[2.245\log_{10}\left(\frac{Pe_l}{30}\right)\right] \tag{31}$$

The liquid fuel studied is *n-decane*. The simplified one-step chemical reaction mechanism is given by

$$C_{10}H_{22} + 15.5O_2 \rightarrow 10CO_2 + 11H_2O \tag{32}$$

The overall reaction rate is given by the following expression[19]:

$$W_{CH}' = A\left(\frac{Y_f\rho_g'}{M_f'}\right)^a\left(\frac{Y_o\rho_g'}{M_o'}\right)^b \exp(-E_A/RT) \tag{33}$$

Initial and Boundary Conditions

Dirichlet boundary conditions are used at the combustor inlet, where mass flow (time-dependent), gas temperature, and species concentration are specified. The inlet pressure is determined by taking the inlet stagnation pressure to be constant. Overall equivalence ratio is specified at the inlet.

At the outlet Neumann boundary conditions are used, where zero gradients of the density, temperature, and species concentration are employed. The short-nozzle approximation at the combustor outlet (entrance to the nozzle) allows the exit Mach number to be constant.[20]

Initially, the gas-phase temperature, velocity, pressure, and species concentration are specified. For the liquid-phase, the droplet radius, location, velocity, and temperature are specified.

Solution Procedure

The numerical solution is based on the modified ICE scheme.[15,16] The salient features of this staggered-grid scheme are advanced time (implicit) treatment of density in the equation of state, of density, and of velocity in the continuity and momentum equations, of temperature and pressure in the energy equation and of density and concentration in the species equation. The continuity and momentum finite-difference equations are combined, the equation of state is introduced, and the resulting equation is solved for the advanced density. Trial runs with various mesh sizes indicated the presence of some numerical diffusion when using a coarse grid. Consequently, a finer grid (201 nodes for 50 cm combustor length) has been employed, and all results presented are grid independent.

Results and Discussion

Results from several cases covering a wide range of parameters are obtained. In all cases, the approach is to start the combustor at time $t = 0$ when the first droplet group is injected. After the combustor reaches a steady operating state at about three times the residence time based on inlet gas velocity, the inlet velocity is perturbed by forcing a sinusoidal cycle with an amplitude of ±20% of the steady velocity. After one cycle, the forced flow ceases and the combustor is free to oscillate. In some other cases, continuous oscillations are imposed on the inlet gas velocity. The parameters survey includes droplet sizes of 15, 25, 50, 75, and 100 μm, overall fuel equivalence ratios of 0.15, 0.3, 0.5, and 0.7, and combustor lengths of 25, 50, 100, and 150 cm. Some runs have

Table 1 Summary of results, overall equivalence ratio = 0.3

r_i (μm)	Result		Max. temp. (K)	Max. pressure (atm)	Frequency (Hz)		Oscillations (±%) Low f			High f		
	Low f	High f			Low	High	p	T	u	p	T	u
				Length = 25 cm								
15	stable	stable	1665	13.1	—	—	0	0	0	0	0	5
25	stable	stable	1620	12.9	—	—	0	0	0	0	0	3
50	stable	unstable	1500	12.5	—	2833	0	0	0	1	3	21
75	stable	stable	1590	13.1	—	1910	0	0	0	0	3	1
100	stable	stable	1425	12.3	—	1420	0	0	0	0	3	3
				Length = 50 cm								
15	stable	stable	1710	13.0	—	801	0	0	0	1	0	3
25	stable	stable	1620	12.9	—	772	0	0	0	2	0	2
50	stable	unstable	1490	12.4	—	756	0	0	0	2	2	20
75	w. unstab.	w. unstab.	1460	12.7	70	729	7	15	6	1	2	7
100	stable	stable	1680	13.2	—	1435	0	0	0	4	4	3
				Length = 100 cm								
25	stable	stable	1630	12.9	—	392	0	0	0	1	0	1
50	stable	unstable	1500	12.6	—	392	0	0	0	2	1	10
75	w. unstab.	unstable	1290	11.4	85	364	3	6	8	2	0	13
100	unstable	unstable	1350	10.6	39	342	10	17	12	2	0	25
				Length = 150 cm								
25	stable	stable	1650	12.9	—	255	0	0	0	1	0	3
50	stable	w. unstab.	1500	12.5	—	247	0	0	0	3	0	9
75	w. unstab.	unstable	1275	11.4	69	213	3	8	8	1	0	13
100	w. unstab.	unstable	1125	10.6	40	212	3	4	9	3	0	12

Note: Classification of stability is based on velocity oscillations as follows:
Stable for $0\% < \Delta u/u < 5\%$.
Weakly unstable for $5\% < \Delta u/u < 10\%$.
Unstable for $10\% < \Delta u/u$.

Table 2 Frequency comparison for OER = 0.3

r_l, μm	r.f.[a] frequency, Hz for lengths, cm			Frequency corresponding to droplet heating time, Hz	τ_p/τ_{dh} for lengths, cm		
	50	100	150		50	100	150
15	820	—	—	1350	1.69	—	—
25	795	405	270	490	0.64	1.25	1.92
50	750	380	255	120	0.16	0.31	0.48
75	755	355	240	55	0.08	0.15	0.26
100	755	350	235	30	0.04	0.09	0.14

[a]Resonant fundamental.

been made with a larger amplitude of perturbation (±35% of the inlet velocity) and these resulted in similar combustor behavior to that for a ±20% perturbation.

Several frequencies of the forcing function are used. After one forced cycle of perturbation of the inlet velocity, in all cases, it is observed that the combustor returns to its natural frequency of oscillation. Hence, it is concluded that when the combustor is free to oscillate, the frequency of oscillation is independent of the frequency of the perturbation function, and, in our results, it is solely determined by the length of the combustor, the droplet size, and the overall equivalence ratio. These results are summarized in Table 1. The natural frequency is found to increase with increasing overall equivalence ratio, decrease with increasing droplet radii, and decrease with decreasing length. Also, this frequency is determined to be very near the fundamental resonant frequency of the combustion chamber. Results for equivalence ratio of 0.3 and 50 cm combustor length are summarized in Table 2. Here, the fundamental resonant frequency is estimated by integrating the temperature profile to obtain the mean speed of sound, and then $f = \bar{a}/(2L)$.

At the lower overall equivalence ratio of 0.3 and for a combustor length of 50 cm, the oscillations, after a cycle of perturbation, dampen and ultimately disappear for lower droplet radii of 15 and 25 μm. Fig. 2 shows velocity and pressure oscillations at different locations along the length of the combustor, for a droplet radius of 25 μm. The oscillations are observed to decay completely (within ±5% of the mean value) in about ten cycles. For the cases of 50- and 75-μm droplets, the startup transient oscillations themselves do not decay completely. In these cases limit cycle behavior is seen, with the magnitude of oscillations dependent upon droplet size. Fig. 3 shows velocity, pressure, and gas flow rate oscillations for the case of 50-μm droplets. Note here that an oscillating-limit-cycle solution results with the magnitude of the velocity oscillations about ±20% of the mean value. The case of 100-μm droplet size is found to be weakly unstable, with relatively small oscillations.

With the overall equivalence ratio increased to 0.5, even the previously stable cases (15- and 25-μm radii droplets) result in weakly oscillating solutions, along with 50-, 75-, and 100-μm cases which are again unstable. At an equivalence ratio of 0.7, all the droplet sizes were found to result in strongly unstable solutions. These trends suggest that the amplitude of the limit cycles increases with equivalence ratios. This trend is similar to recent experimental observations[21] indicating large

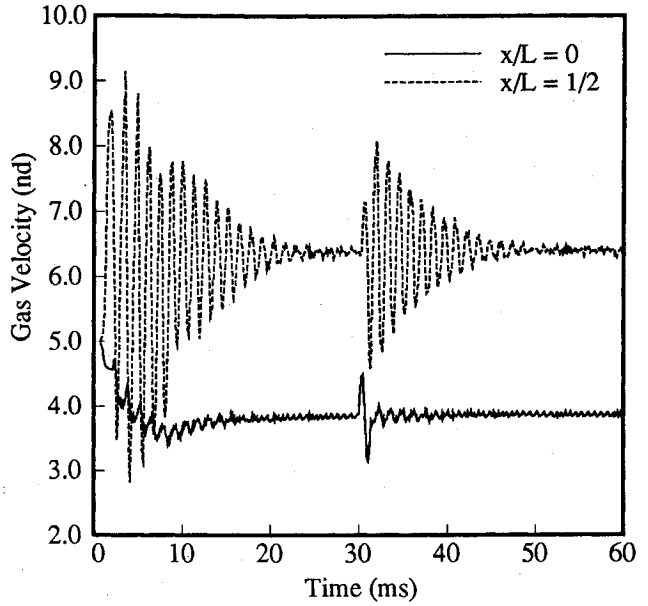

Fig. 2a Velocity: For L = 50 cm, OER = 0.3, r_i = 25 μm.

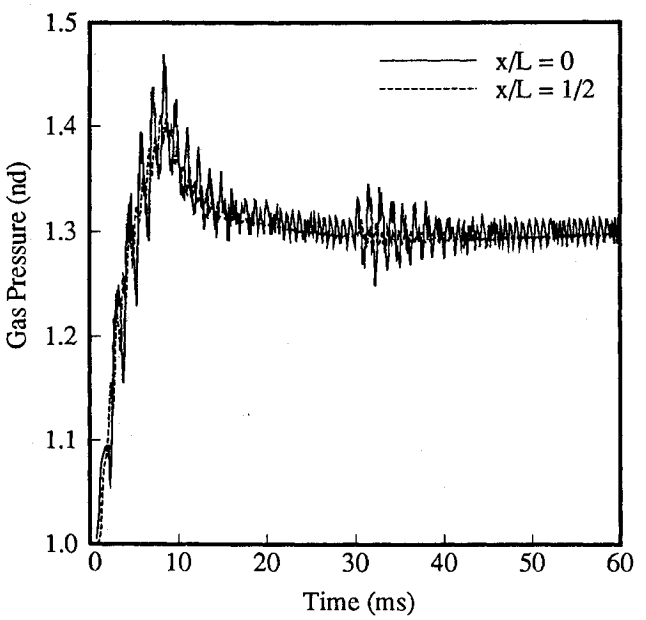

Fig. 2b Pressure: For L = 50 cm, OER = 0.3, r_i = 25 μm.

pressure oscillations for higher equivalence ratios, typically over 0.6. Also here, the oscillations start showing overtones and the frequency rises.

The effect of increasing length of the combustor is to cause a proportionate decrease in the natural frequency. The amplitude of the oscillations decreases somewhat for the 50-μm droplet cases, in varying the combustor length from 50 cm to 100 cm. At 150-cm length, the 50-μm case becomes almost stable. However, this is not true for the 100-μm droplet case, where the amplitude of the oscillations first increases and then decreases, with increasing combustor length.

Evidence of standing pressure waves in the combustion chamber has been observed. See Fig. 4, which shows the pressure profile in the combustion chamber as a function of time.

In Fig. 5, a comparison of the integrated vaporization and burning rates is provided. It is clear that the vaporization and burning rates are very close in magnitude and, hence, vaporization is rate controlling. The different asymptotic values (about 10% difference) of the vaporization and burning rates in Fig. 5 result from numerical error associated with integrating the step-like values of the rates.

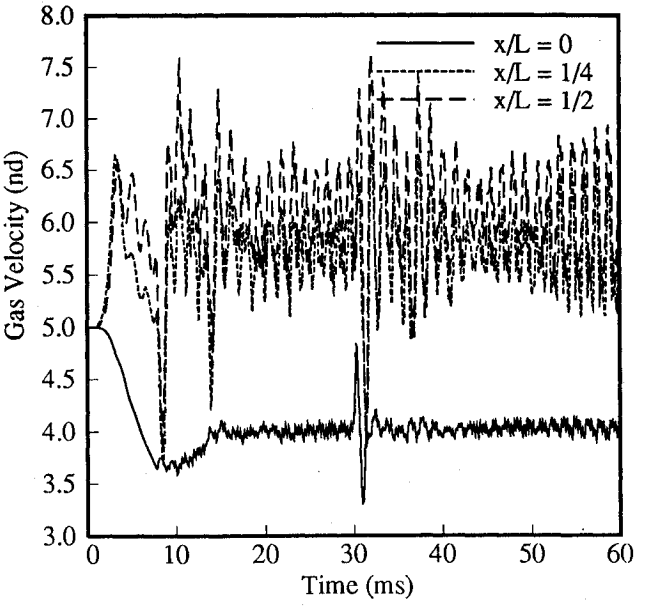

Fig. 3a Velocity: For L = 50 cm, OER = 0.3, r_i = 50 μm.

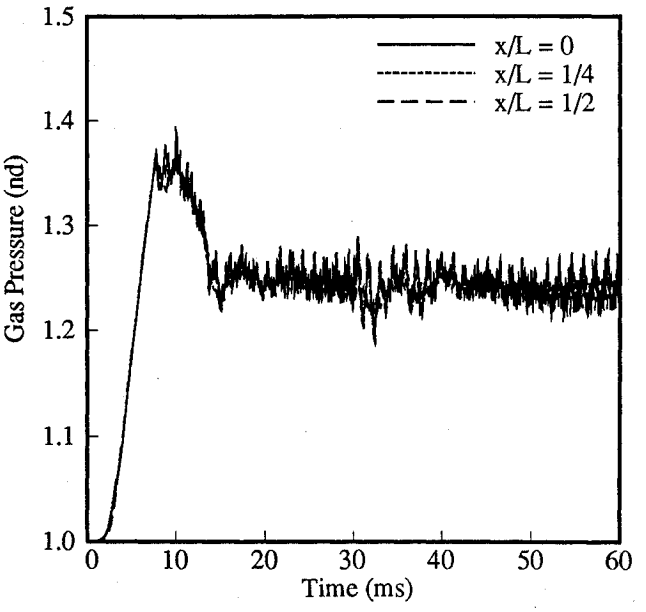

Fig. 3b Pressure: For L = 50 cm, OER = 0.3, r_i = 50 μm.

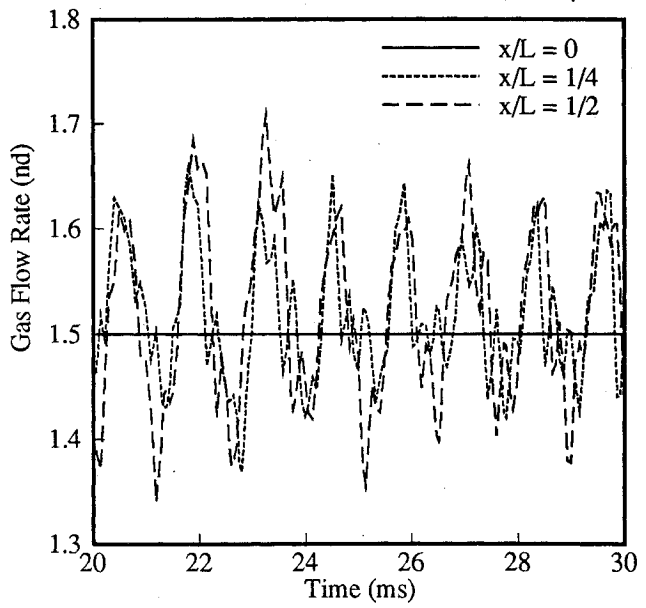

Fig. 3c Gas flow rate: For L = 50 cm, OER = 0.3, r_i = 50 μm.

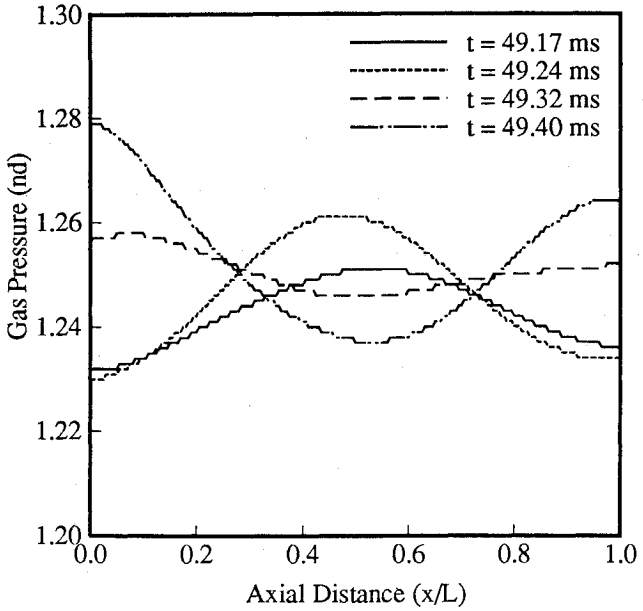

Fig. 4 Pressure waves in the combustor: For L = 25 cm, OER = 0.3, r_i = 25 μm.

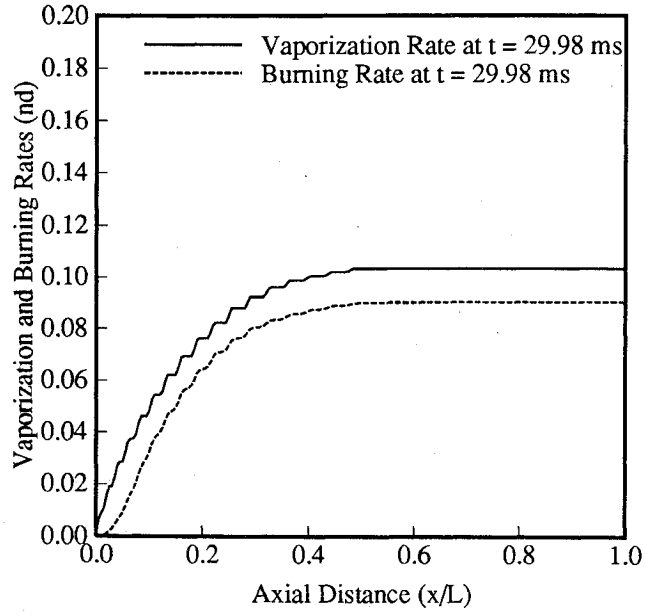

Fig. 5 Vaporization and burning rates: For L = 50 cm, OER = 0.3, r_i = 50 μm.

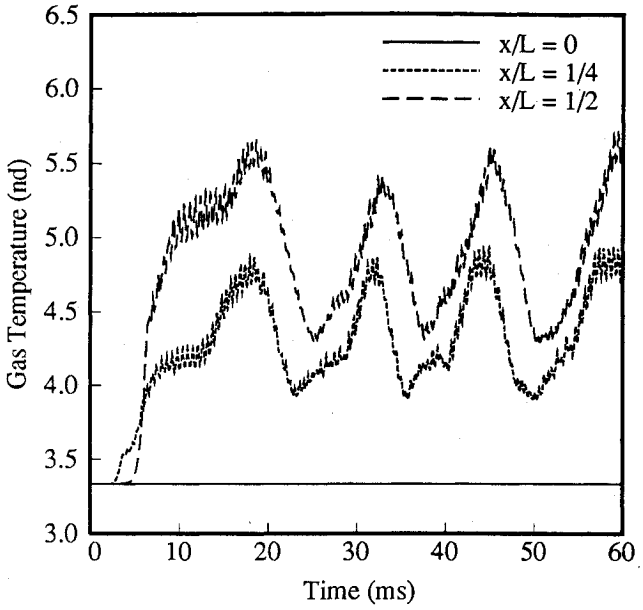

Fig. 6a Temperature: For L = 50 cm, OER = 0.3, r_i = 75 μm.

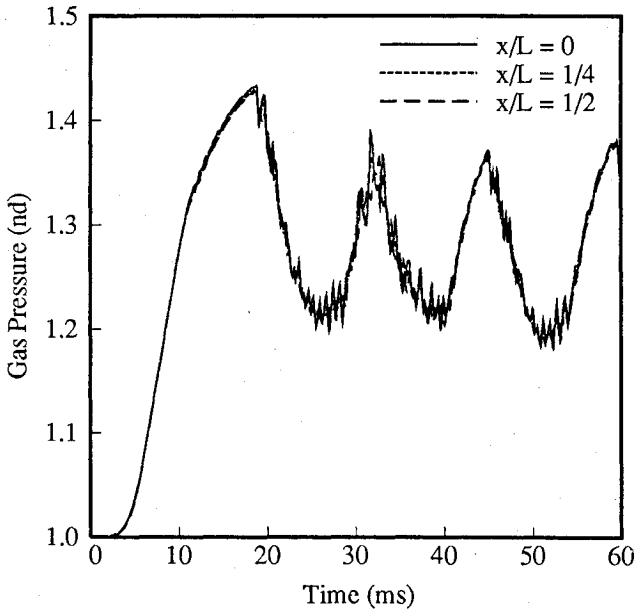

Fig. 6b Pressure: For L = 50 cm, OER = 0.3, r_i = 75 μm.

Also for the 75-μm case, the presence of a "dark" region is clearly observed, which is convected downstream with the gas velocity, as shown in Fig. 6 which gives temperature and pressure oscillations for an equivalence ratio of 0.3. The dark region indicates the presence of gases at lower temperatures. This is in accordance with Crocco and Cheng[1] who explain this as local temperature oscillations (and thus local entropy oscillations) which propagate at the speed of mass motion. The amplitude of the temperature oscillations associated with these waves is very large. Similar behavior is observed to a smaller extent with 50-μm droplet radius and to a similar extent with 100-μm droplet radius at equivalence ratios of 0.5 and 0.7 (See Fig. 7.)

When continuous oscillations are imposed on the inlet gas velocity, resonance occurs if the forcing function frequency is close to the natural frequency of the combustor. The results for these cases, where the oscillatory perturbations on the inlet gas velocity were continued for ten cycles, is shown in Fig. 8. The rate at which these oscillations grow is dependent upon the frequency of the forcing function and the droplet radius.

Three distinct frequencies of oscillations, which may exist simultaneously, are seen in our results. The one prevalent frequency is the fundamental resonant frequency of the combustor, which is of order of 800 Hz. This frequency is always present in cases which are unstable. A lower frequency of about 100 Hz is also observed for larger (i.e. 75 and 100 μm) droplets. This frequency corresponds to the gas residence time in the combustor. And at higher equivalence ratios, we see frequencies of order of few thousand Hz, which correspond to the injection frequency of the droplets. Note that the injection frequency is an artificial numerical result. Figure 9 shows the case of 50-μm droplets at an equivalence ratio of 0.5, for which the fundamental resonant frequency is about 865 Hz and the injection frequency is about 3400 Hz. Here, we can see the primary mode of oscillation (fundamental) which is at 870 Hz. We also see the injection frequency and some other large frequencies of a few thousand Hertz; these

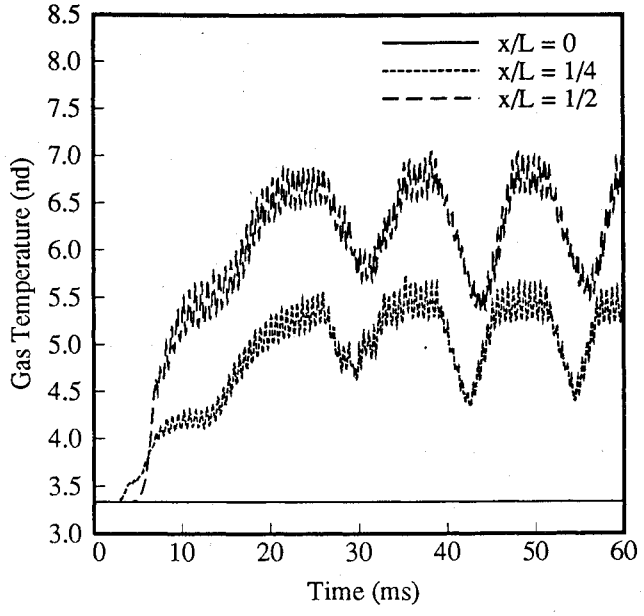

Fig. 7a Temperature: For L = 50 cm, OER = 0.5, r_i = 100 μm.

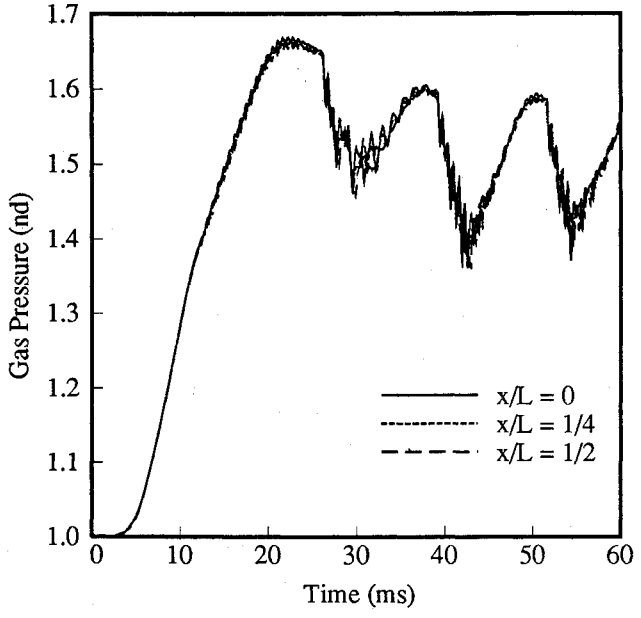

Fig. 7b Pressure: For L = 50 cm, OER = 0.5, r_i = 100 μm.

possibly result from the coupling of acoustic and injection frequencies. Also in Figs. 6 to 7, along with low-frequency oscillations, which are of the order of 100 Hz, we see smaller oscillations corresponding to twice the acoustic frequency or about 1800 Hz.

These results are summarized in Figs. 10 to 13 which map the domains of stable/unstable combustion with the droplet radius, the combustor length, and the overall equivalence ratio as the parameters. Figure 10 shows the domain as determined by the droplet radius and the combustor length. With increase of the droplet size for a fixed combustor length, the combustion passes from stable to unstable and back to stable. Also evident is the effect of the combustor length. At the lower droplet radius of 50 μm, increasing length moves the combustion process from unstable to stable, whereas the opposite is true at the higher droplet radius of 100 μm. In Table 2, we have estimated the characteristic time for droplet heating and thus determined the characteristic frequency corresponding to droplet heating time. Here, the characteristic time for droplet heating for the *n-decane* droplets burning in

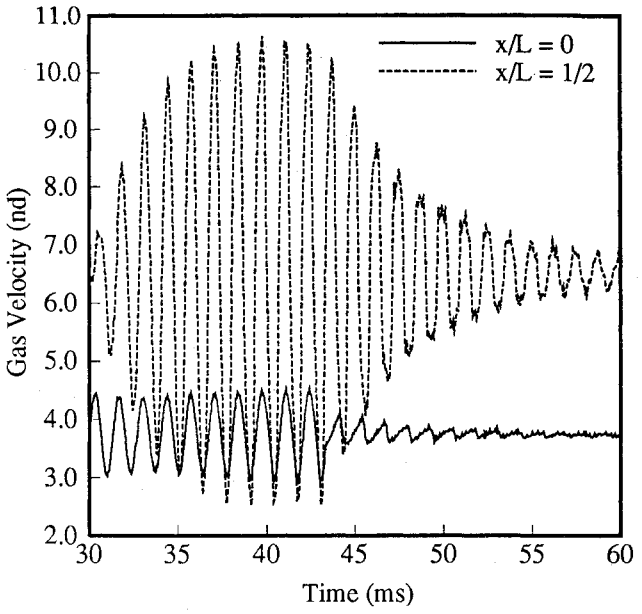

Fig. 8 Continuously forced gas velocity perturbations for ten cycles: For L = 50 cm, OER = 0.3, r_i = 15 μm.

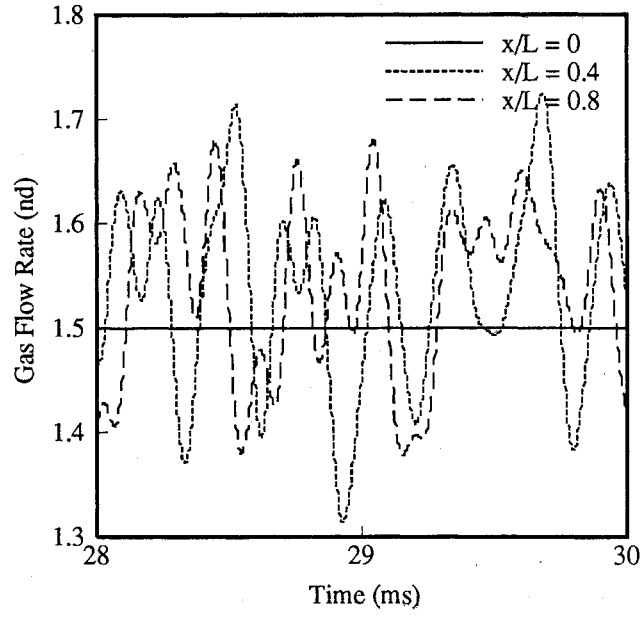

Fig. 9 Gas flow rate: For L = 50 cm, OER = 0.3, r_i = 50 μm.

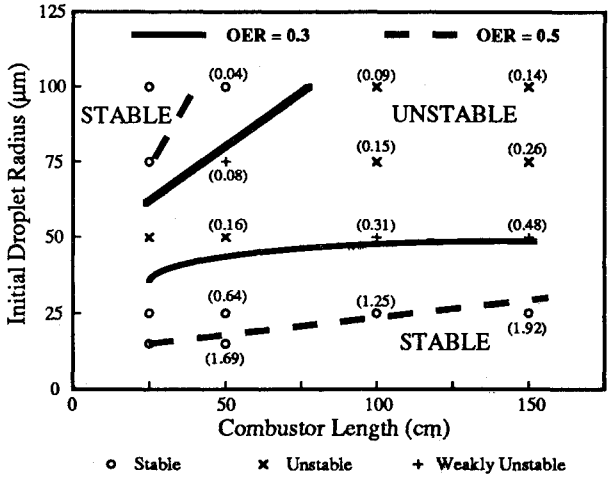

Fig. 10 Domain of stable/unstable operation: Droplet radius and combustor length. Points shown correspond to OER = 0.3. Numbers in parenthesis indicate τ_p/τ_{dh}.

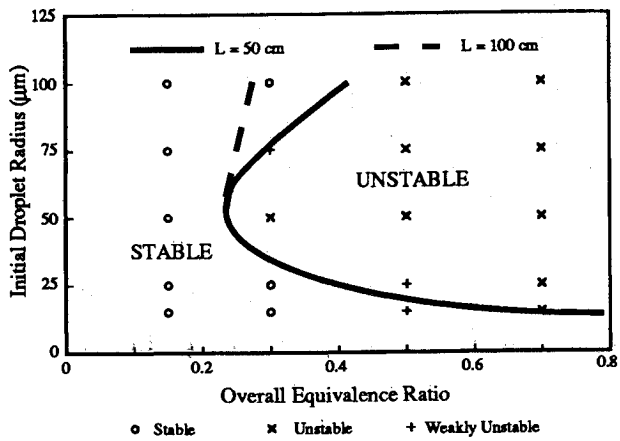

Fig. 11 Domain of stable/unstable operation: Droplet radius and equivalence ratio. Points shown correspond to L = 50 cm.

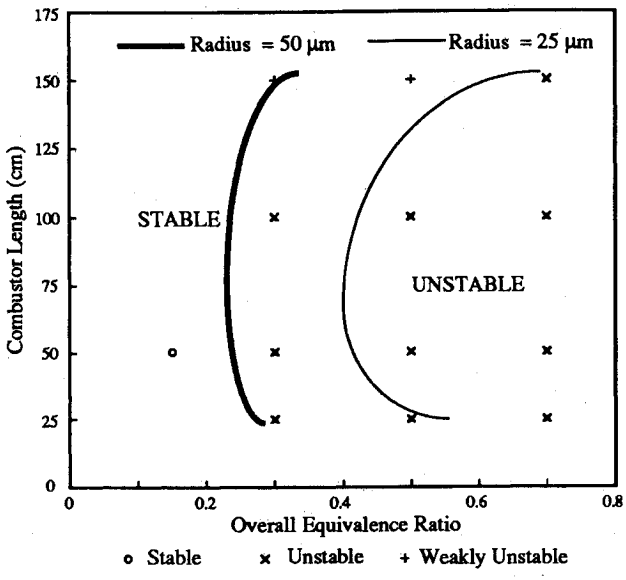

Fig. 12 Domain of stable/unstable operation: Combustor length and equivalence ratio. Points shown correspond to r_i = 50 μm.

1000 K air at 10 atm pressure is estimated as $\tau_{dh} \sim (\rho_l C_{p_g}/\lambda_g) r_l^2 \approx d_l^2/1.22 * 10^{-06}$ (m^2 − s/m^2). With fixed combustor length and increasing droplet radius, the characteristic time associated with the droplet heating increases. In some intermediate droplet radius range, it matches with the characteristic acoustic period so that the droplet vaporization can excite the acoustic modes. At higher droplet radii (75 and 100 μm), the low-frequency oscillations begin to get excited and this phenomenon is explained later. The characteristic time associated with the acoustic frequency, $\tau_a \sim L$, and this explains the increase in the stable region on increasing the combustor length. Also shown in Table 2 and Fig. 10 is the ratio of characteristic times for the oscillations to that for the droplet heating (τ_p/τ_{dh}). For unstable high-frequency cases, τ_p/τ_{dh} is in a range from 0.08 to 0.48. The points in the center of the unstable range vary between 0.14 and 0.16. Therefore, we take 0.15 as the most unstable value of the ratio. Tong and Sirignano,[8] in their study of response of a vaporizing droplet in unstable combustor report a maximum gain occurring for oscillations of frequency 200 Hz for 100-μm droplets. Using a characteristic frequency of 30 Hz for 100-μm droplet heating (from Table 2), we obtain τ_p/τ_{dh} = 0.15, for the Tong-Sirignano calculation, which reinforces our result.

Figure 11 shows the domain as determined by the droplet radii and the overall equivalence ratio. The domain for unstable operation becomes larger at higher equivalence ratios, as the overtones get excited. The situation is further complicated by the interaction of the simulated injection process. For a fixed rate of injected fuel, the combustion process passes from stable to unstable at lower droplet radii, and again becomes stable at higher droplet radius. Figure 12 shows the stability limits as a function of the combustor length and the overall equivalence ratio. For a given droplet radius, the combustion passes from a stable to an unstable region with increase in the equivalence ratio. In Fig. 13, we isolate the low-frequency oscillations from the high-frequency ones. The figure shows that the low-frequency oscillations are important only in the cases of higher droplet radii. Also shown in the figure is the ratio of characteristic times for residence, taken as $\tau_f = 2L/u_{g,\text{inlet}}$, to the droplet heating time. It is inferred that, to excite the low-frequency modes, the characteristic time for the liquid droplet heating has to correspond to the residence time, or $\tau_f/\tau_{dh} \approx 1.0$.

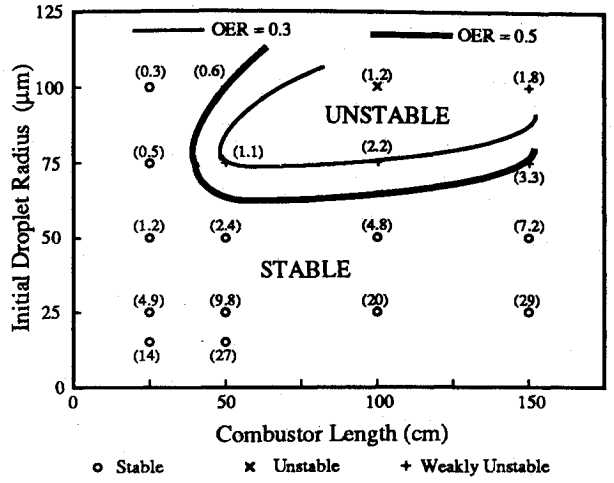

Fig. 13 Domain of stable/unstable operation for low frequency oscillations only: Droplet radius and combustor length. Points shown correspond to OER = 0.3. Numbers in parenthesis indicate τ_f/τ_{dh}.

In our calculations, the Mach number at the combustor exit is fixed at approximately 0.08. Some runs with a higher Mach number indicate a reduction in the amplitude of oscillations. Finally, it is noted that a one-dimensional study cannot resolve transverse transport and mixing. Hence, the related important issues of multidimensional geometry, turbulent transport, vortex shedding, and their interactions with the acoustic oscillations cannot be studied in this model. Other straightforward extensions of the work include using poly disperse and/or multicomponent sprays.

Conclusions

Certain general conclusions can be drawn.

1) Vaporization is rate controlling in the one-dimensional simulation where turbulent mixing and transverse transport are not considered.

2) The combustion process can occur in either a stable or unstable mode. In the unstable mode, limit-cycle behavior of pressure, temperature, velocity, and gas-phase mass flow rate will occur. The magnitude of these limit-cycle oscillations is determined by the combustor geometry, spray characteristics and the overall equivalence ratio.

3) Low-frequency or entropy oscillations result when the characteristic time for droplet heating is close to that for the gas residence. High-frequency oscillations result when the ratio of characteristic time for period of oscillation to droplet heating is close to 0.15.

4) The frequency of free oscillations is very close to the fundamental resonant frequency of the combustor, at lower equivalence ratios. At higher equivalence ratios, overtones are present.

5) The frequency of the initial perturbation function has a small effect on the combustor oscillations. When the forcing

function is removed, the combustor oscillations return to their natural frequency within a few cycles of oscillation.

6) In cases where the damping of excited acoustic oscillations occurs, the excitations tend to dampen in about 10 cycles.

7) The variation of droplet size, for the same equivalence ratio and combustor length, has a profound effect on the combustor stability. A range of droplet radii for which the combustion is unstable is observed. Below and above this range of droplet size, no limit-cycle behavior is present. This indicates the importance of spray combustion.

8) An intermediate range also exists for combustor length, like the droplet radii, where the combustor operation is unstable.

9) Increasing the equivalence ratio enlarges the domain of unstable operation. All droplet radii and combustor length cases, in the range of the calculations, are unstable for the equivalence ratio of 0.7.

10) When the inlet gas velocity is continuously excited, resonance occurs for an excitation frequency close to the combustor natural frequency.

Acknowledgment

The work was supported by a Grant N00014-85-K0658 from the Office of Naval Research, with K. Ellingsworth and G. Roy serving as technical monitors. The preliminary work of G. Riva on this project is also acknowledged.

References

[1]Crocco, L., and Cheng, Sin-I, *Theory of Combustion Instability in Liquid Propellant Rocket Motors*, Butterworths Scientific Publications, 1956.

[2]Harrje, D. T., and Reardon, F. A. (editors), *Liquid Propellant Rocket Combustion Instability*, NASA SP-194, 1972.

[3]Strahle, W. C., "Periodic Solutions to a Convective Droplet Burning Problem: The Stagnation Point," *Tenth International Symposium on Combustion*, The Combustion Institute, 1965, pp. 1315–1325.

[4]Strahle, W. C., "Unsteady Reacting Boundary Layer on a Vaporizing Flat Plate," *AIAA Journal*, Vol. 3, No. 6, 1965, pp. 1195–1198.

[5]Priem, R. J., and Heidmann, M. F., "Propellant Vaporization as a Design Criterion for Rocket Engine Combustion Chambers," NASA TR R-67, 1960.

[6]Heidmann, M. F., and Wieber, P. R., "Analysis of Frequency Response Characteristics of Propellant Vaporization," NASA TN D-3749, 1966.

[7]Sirignano, W. A., "Fuel Droplet Vaporization and Spray Combustion Theory," *Progress in Energy and Combustion Science*, Vol. 9, 1983, pp. 291–322.

[8]Tong, A. Y., and Sirignano, W. A., "Oscillatory Vaporization of Fuel Droplet in Unstable Combustor," *Journal of Propulsion and Power*, Vol. 5, No. 3, 1989, pp. 257–261.

[9]Awad, E., and Culick, F. E. C., "On the Existence of Stability of Limit Cycles for Longitudinal Acoustic Modes in a Combustion Chamber," *Combustion Science and Technology*, Vol. 46, 1986, pp. 195–222.

[10]Crump, J. E., Schadow, K. C., Yang, V., and Culick, F. E. C., "Longitudinal Combustion Instability in Ramjet Engines: Identification of Acoustic Modes," *Journal of Propulsion and Power*, Vol. 2, No. 2, 1986, pp. 105–109.

[11]Yang, V., and Culick, F. E. C., "Analysis of Low Frequency Combustion Instabilities in a Laboratory Ramjet Combustor," *Combustion Science and Technology*, Vol. 45, 1986, pp. 1–25.

[12]Kailasanath, K., Gardner, J. H., Boris, J. P., and Oran, E. S., "Numerical Simulations of Acoustic-Vortex Interactions in a Central-Dump Ramjet Combustor," *Journal of Propulsion and Power*, Vol. 3, No. 6, 1987, pp. 525–533.

[13]Hedge, U. G., Reuter, D., Daniel, B. R., and Zinn, B. T., "Flame Driving of Longitudinal Instabilities in Dump Type Combustors," *Combustion Science and Technology*, Vol. 55, 1987, pp. 125–138.

[14]Abramzon, B., and Sirignano, W. A., "Droplet Vaporization Model for Spray Combustion Calculations," *International Journal Heat Mass Transfer*, Vol. 32, No. 9, 1989, pp. 1605–1618.

[15]Harlow, F. H., and Amsden, A. A., "A Numerical Fluid Dynamics Calculation Method for All Flow Speeds," *Journal of Computational Physics*, Vol. 8, 1971, pp. 197–213.

[16]Westbrook, C. K., and Chase, L. L., "A One-Dimensional Combustion Model," UCRL-52297, Lawrence Livermore Laboratory, Livermore, CA, 1977.

[17]Sirignano, W. A., "The Formulation of Spray Combustion Models: Resolution Compared to Droplet Spacing," *Journal of Heat Transfer*, Vol. 108, 1986, pp. 633–639.

[18]Clift, R., Grace, J. R., and Weber, M. E., *Bubbles, Drops and Particles*, Academic Press, New York, 1978, p. 121.

[19]Westbrook, C. K., and Dryer, F. L., "Chemical Kinetic Modelling of Hydrocarbon Combustion," *Progress in Energy and Combustion Science*, Vol. 10, 1984, pp. 1–57.

[20]Crocco, L., and Sirignano, W. A., "Effect of the Transverse Velocity Component on the Nonlinear Behavior of Short Nozzles," *AIAA Journal*, Vol. 4, No. 8, 1966, pp. 1428–1430.

[21]Yu, K., Keanini, R., Bauwens, L., and Daily, J., "Low Frequency Pressure Oscillations in a Model Ramjet Droplet Combustor, The Nature of Frequency Selection," AIAA 27th Aerospace Sciences Meeting, AIAA Paper 89-0623, Reno, NV, 1989.